CrossMark

# Linear diffraction analysis for optimisation of the three-float multi-mode wave energy converter M4 in regular waves including small arrays

L. Sun[1] · P. Stansby[2] · J. Zang[1] · E. Carpintero Moreno[2] · P. H. Taylor[3]

**Abstract** A general frequency domain dynamic model based on the DIFFRACT code has been developed to predict the motion and power generation of the three-float multi-mode wave energy converter M4, modelled as a two-body problem. The machine has previously been shown experimentally and numerically to have broad-band high capture widths for the range of wave periods typical of offshore sites. The float sizes increase from bow to stern; the bow and mid float are rigidly connected by a beam and the stern float is connected by a beam to a hinge above the mid float where the rotational relative motion is damped to absorb power. The floats are approximately half a wavelength apart so the float forces and motion in antiphase generate relative rotation. Here regular waves representative of swell are investigated and the model is shown to give accurate predictions of experimental results for motion and power for small wave heights

and motion which are representative of operational conditions. A linear damper is used to model the power take-off. Without changing the float geometry or the hinge position, adjusting the linear damping factor for each frequency is shown to increase the power by up to three times the experimental value, with a maximum close to the theoretical value for a single float. Increasing the height of the hinge point above the mid float increases the power for the higher periods but can reduce power at lower periods. Since float motion can be quite large, this result can only be indicative of qualitative trends. The effect of small rows has been investigated, up to five machines, and it is shown in particular how the performance of wave energy devices in a row was affected by the multi-body interactions and wave directions. These results are important since the optimum damping factor is shown to be frequency dependent, and increase power generation by up to three times. Furthermore, hydrodynamic interference between M4 machines in a row may significantly increase the power generation when appropriate spacings are chosen.

**Keywords** Wave energy converter · Hydrodynamic interaction · Power take-off · Power absorption · Optimisation · Array

✉ P. Stansby
p.k.stansby@manchester.ac.uk

L. Sun
l.sun@bath.ac.uk

J. Zang
j.zang@bath.ac.uk

E. Carpintero Moreno
efrain.carpinteromoreno@manchester.ac.uk

P. H. Taylor
paul.taylor@eng.ox.ac.uk

[1] WEIR Research Unit, Department of Architecture and Civil Engineering, University of Bath, Bath BA2 7AY, UK

[2] School of Mechanical, Aerospace and Civil Engineering, University of Manchester, Manchester M13 9PL, UK

[3] Department of Engineering Science, University of Oxford, Parks Road, Oxford OX1 3PJ, UK

## 1 Introduction

Many devices have been considered for the conversion of ocean wave motion into electricity, see for example, the reviews of Falcão (2010), Wolgamot and FitzGerald (2015) and Babarit (2015). The wave resource is greatest offshore in deeper water and here we consider a three-float moored system with high capture width known as M4 (Stansby et al. 2015a, b). The floats increase in size from bow to stern giving a range of natural periods in heave and pitch, providing

**Fig. 1** Main dimensions of the laboratory-scaled model (unit: m)
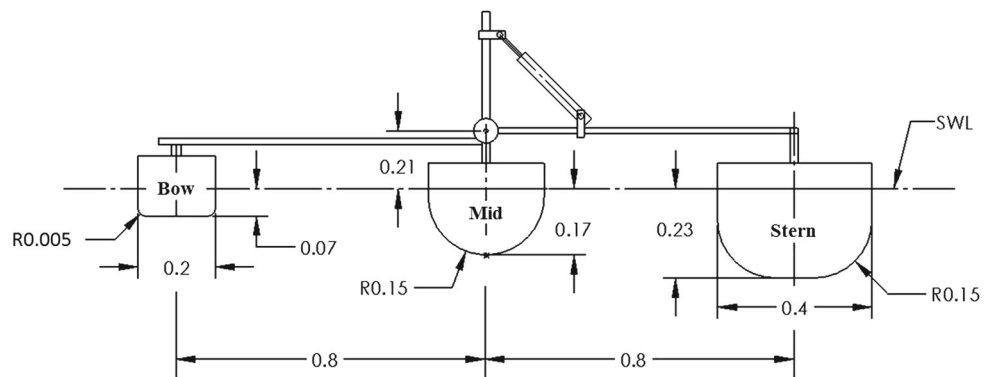


a broad-band response so that significant power generation across the ranges of wave periods occurring at a typical site may be obtained. The distance between floats is about half a typical wavelength so that forces and float motions are predominantly in anti-phase. With the progression down wave from small to medium to large floats, the device naturally heads into the wave direction. The diagram in Fig. 1 with dimensions for laboratory scale (approximately 1:70 of field scale for swell waves of 10 s period on the open sea) shows the bow and mid float rigidly connected by a beam and the stern float connected by a beam to the hinge point above the mid float on a column on the centreline axis.

The mid and stern floats have rounded bases with the same radius of curvature (hemispherical for the mid float) to minimise drag. This has been demonstrated for heave using CFD (Stansby et al. 2015c). This design has been investigated experimentally at two different scales (approximately 1:8 and 1:40 for irregular wind waves with 7 s peak period) in different basins and similar non-dimensional results based on Froude scaling have been obtained, in this case for floats with flat bases (Stansby et al. 2015b). Some numerical analysis has also been undertaken based on linear diffraction coefficients in the time domain (Stansby et al. 2015a) and in the frequency domain with a general structural dynamic model (Eatock Taylor et al. 2016). The latter showed four natural modes of relative pitch response, three within the range of typical wave periods (after appropriate scaling). The former showed that heave and surge forcing generated most of the power, although surge individually has no resonance condition but provides large anti-phase moments about the hinge. Clearly the system is quite complicated and there is considerable scope for optimisation, e.g., float dimensions, hinge point, power take-off characteristics. It is also important to consider interactions in arrays. A validated efficient general numerical model is thus highly desirable. Power generation in broad-banded irregular waves is generally important but power generation in almost regular swell waves can also be significant. Analysis with regular waves is also beneficial for basic understanding of the system response and power generation resulting from one input frequency. This is undertaken

here using the DIFFRACT code (Sun et al. 2015) for frequency domain multi-body dynamic analysis. All six modes of motion are included for each body with all wave/body interactions. Second-order forcing is also available although not used here. The body motions are coupled in a multi-body formulation. This is, thus, a powerful tool for analysing complex wave/body interactions.

First the numerical method is validated against regular wave experiments with an almost linear damper representing the power take-off. Some optimisation is then undertaken varying the linear damping constant and the hinge point position along the mid body axis; the body dimensions are not varied in this study. Finally rows of up to five devices are considered.

## 2 Numerical model

### 2.1 Multi-body dynamic model for wave energy converters

To derive the multi-body dynamic model for wave energy converters, we start from the equations of motion for multiple floating bodies without any mechanical connections which can be written in the following form (Sun et al. 2012)

$$\left[-\omega^2(M + A_H(\omega)) - i\omega(B + B_H(\omega)) + (C + C_H)\right]\{\xi(\omega)\} = \{f_{\text{ex}}(\omega)\} \quad (1)$$

in which, $\{f_{\text{ex}}(\omega)\}$ on the right hand side represents the linear wave excitation forces and moments which are related to the geometries of floating bodies and the incident waves (with water depth $d$, wave height $H$, wave period $T$ and wave incident angle $\beta$ as shown in Fig. 2). Unknowns $\{\xi(\omega)\}$ on the left hand side include all complex motions of multiple rigid modules. Both $\{f_{\text{ex}}(\omega)\}$ and $\{\xi(\omega)\}$ are frequency dependent complex vectors which include $6N$ components for a system consisting of $N$ bodies. The matrix $M$ is the rigid body mass matrix for the $N$ bodies, while $B$ and $C$ are external

**Fig. 2** Top view of wave energy converter M4 showing definition of wave incident angle $\beta$
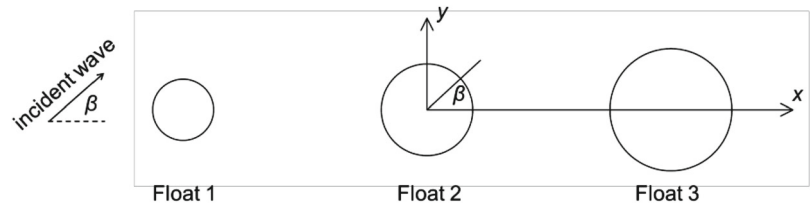


linear damping and stiffness matrices. Matrix $C_H$ represents the hydrostatic restoring coefficients. Matrices $A_H(\omega)$ and $B_H(\omega)$ are the added mass and radiation damping matrices that are related to the radiation forces due to the body motions (determined by the geometries of bodies). In present analysis, the excitation forces and moments $\{f_{\text{ex}}(\omega)\}$, and hydrodynamic coefficients $A_H(\omega)$ and $B_H(\omega)$ are evaluated by the computer program DIFFRACT based on the linear potential flow theory.

Eq. (1) can be written in a matrix form as

$$[K]\{\xi\} = \{f_{\text{ex}}\} \qquad (2)$$

To account for the mechanical connections between the floats (hinges in this case) of a WEC, the augmented equations of motions based on Lagrangian dynamics (Shabana 2010) can be derived. The technique of Lagrange multipliers $\{\lambda\}$ is introduced to define the generalized constraint forces and the motion equations are written as (Sun et al. 2012)

$$\begin{bmatrix} K & D^T \\ D & 0 \end{bmatrix} \begin{Bmatrix} \xi \\ \lambda \end{Bmatrix} = \begin{Bmatrix} f_{\text{ex}} \\ 0 \end{Bmatrix} \qquad (3)$$

where $D$ is a constraint matrix, which defines the kinematic connectivity between the floating modules in a WEC. For two floating bodies connected by a planar hinge (only relative pitch motion is allowed), there are five constraints to be defined and the transpose of the constraint matrix $D^T$ has the following form (Sun et al. 2011).

$$D^T_{12 \times 5} = \begin{bmatrix} 1 & 0 & 0 & 0 & 0 \\ 0 & 1 & 0 & 0 & 0 \\ 0 & 0 & 1 & 0 & 0 \\ 0 & -(z_1 - z_{c1}) & y_1 - y_{c1} & 1 & 0 \\ z_1 - z_{c1} & 0 & -(x_1 - x_{c1}) & 0 & 0 \\ -(y_1 - y_{c1}) & x_1 - x_{c1} & 0 & 0 & 1 \\ -1 & 0 & 0 & 0 & 0 \\ 0 & -1 & 0 & 0 & 0 \\ 0 & 0 & -1 & 0 & 0 \\ 0 & z_1 - z_{c2} & -(y_1 - y_{c2}) & -1 & 0 \\ -(z_1 - z_{c2}) & 0 & x_1 - x_{c2} & 0 & 0 \\ y_1 - y_{c2} & -(x_1 - x_{c2}) & 0 & 0 & -1 \end{bmatrix} \qquad (4)$$

Here $(x_{c1}, y_{c1}, z_{c1})$ and $(x_{c2}, y_{c2}, z_{c2})$ are the co-ordinates of the centres of gravity (CoG) of each body in the dynamic model, as shown in Table 1, and $(x_1, y_1, z_1)$ is the location of

**Table 1** Mass distribution and inertia for rounded base configuration with origin at hinge point

| | Mass (kg) | $X_{\text{CoG}}$(m) | $Z_{\text{CoG}}$(m) |
|---|---|---|---|
| Float 1 | 2.00 | −0.8 | −0.195 |
| Beam float 1 to 2 | 0.20 | −0.5 | −0.094 |
| Float 2 | 3.28 | 0.0 | −0.254 |
| Beam float 2 to 3 | 0.56 | 0.5 | −0.0 |
| Float 3 | 3.97 | 0.8 | −0.252 |
| Actuator | 0.19 | 0.16 | 0.16 |
| Ballast float 2 | 5.00 | 0.0 | −0.363 |
| Ballast float 3 | 19.0 | 0.8 | −0.363 |
| Combined floats 1 and 2 | 10.1 | −0.169 | −0.281 |
| Combined float 3 | 24.0 | 0.793 | −0.330 |
| Inertia $I_{yy}$ (pitch) about hinge floats 1 and 2 combined | 2.40 kg m$^2$ | | |
| Inertia $I_{yy}$ (pitch) about hinge float 3 | 18.39 kg m$^2$ | | |
| Inertia $I_{xx}$ (roll) about hinge floats 1 and 2 combined | 1.06 kg m$^2$ | | |
| Inertia $I_{xx}$ (roll) about hinge float 3 | 3.26 kg m$^2$ | | |
| Inertia $I_{zz}$ (yaw) about hinge floats 1 and 2 combined | 1.49 kg m$^2$ | | |
| Inertia $I_{zz}$ (yaw) about hinge float 3 | 15.8 kg m$^2$ | | |

hinge which is at (0.0, 0.0, 0.21 m) in the following analysis for the single device as shown in Fig. 1, with the co-ordinate origin at the undisturbed water line on the mid float centre-line.

When PTOs are modelled as linear rotational dampers, the moments introduced by PTOs can be calculated in the frequency domain, as

$$f_{\text{PTO}}(\omega) = -B_d \dot{\theta}_r = i\omega B_d \theta_r \qquad (5)$$

where $\theta_r$ is the complex relative rotation between the rigid modules in a WEC and $B_d$ is the damping factor. For a two-body system with a planar hinge connection, $\theta_r = \xi_{11} - \xi_5$. Here $\xi_1$ to $\xi_6$ denote 6 degrees of motions of body 1 and $\xi_7$

to $\xi_{12}$ are for body 2 in the system. Note in this system the bow and mid floats count as single body 1.

The corresponding coefficients of the complex relative rotations $\theta_r$ can be absorbed into the matrix $K$ in Eq. (3) to account for the effect of PTOs. The equations of motion for the multiple float system containing PTOs become

$$\begin{bmatrix} K_2 & D^T \\ D & 0 \end{bmatrix} \begin{Bmatrix} \xi \\ \lambda \end{Bmatrix} = \begin{Bmatrix} f_{ex} \\ 0 \end{Bmatrix} \tag{6}$$

The mass and inertia of floats, damping moments of PTO, hydrostatic and radiation forces have been incorporated in matrix $K_2$. There is no external damping and the effect of mooring forces is assumed to be small in following analyses ($B = 0$ and $C = 0$).

Equation (6) can provide a clear approach to optimisations of WECs with interconnected floats. On the right hand side of the Eq. (6), $\{f_{ex}(\omega)\}$ are the only external driving forces/moments in this dynamic system. So the process of optimisation can be implemented in two stages. In the first stage, the emphasis can be put on the dynamic analysis considering the optimisations of PTOs and mechanical connections, and in the second stage on the hydrodynamic characteristics of floats. We only consider the first stage in this study.

## 2.2 Capture width and capture width ratio of WECs in regular waves

Under the assumption of PTOs represented by a linear rotational damper, the mean power absorbed in regular waves at frequency $\omega$ can be written as (Mei et al. 2005)

$$P_c = \frac{1}{2}\omega^2 B_d |\theta_r|^2 \tag{7}$$

In regular waves of amplitude $A_i$, the mean incident power per unit width of wave front is

$$P_i = \frac{1}{2}\rho g A_i^2 c_g \tag{8}$$

where $c_g$ is the group velocity of the wave at frequency $\omega$ and corresponding wave number is $k$. In water of depth $d$, $\omega^2 = gk \tanh(kd)$ and $c_g = [1 + 2kd/\sinh(2kd)]\,\omega/2k$. From Eq. (8), it can be seen that $P_i$ will become larger with longer waves for constant wave amplitude $A_i$.

To indicate the power absorption capability of any WEC, the capture width (Falnes 2002) can be defined as

$$CW = \frac{P_c}{P_i} \tag{9}$$

In the present analysis, the capture width ratio (CWR) is defined as

$$CWR = \frac{P_c}{P_i L} \tag{10}$$

where L is the wave length at frequency $\omega$. Comparing Eq. (7) with Eq. (8), it is obvious that the capture width ratio (CWR) is independent of the wave amplitude as long as the WEC is linear. The capture width ratio CWR defined in Eq. (10) may be related to the theoretical maxima for axisymmetric point absorbers, e.g., Falnes (2002), and simplifies scaling up to full scale field conditions.

### 2.3 Interaction factor of WECs in arrays

The interaction $q$-factor is a simple indicator that shows the effect of wave interaction on power absorption of WECs in arrays (Babarit 2013). It is usually defined as the ratio of the total power of the array to the total power from the same number of identical devices each operating in isolation in the same wave field and $q = P_{c,\text{array}}/(N_{\text{array}} P_{c,\text{isolated}})$ (Here $N_{\text{array}}$ is the number of identical devices in the array). However, the traditional $q$-factor hides the real amount of absorbed power of device and large $q$-factor does not always imply significant improvement in the performance (Babarit 2010). We redefine the $q$-factor as

$$q = \frac{P_{c,\text{array}} - N_{\text{array}} P_{c,\text{isolated}}}{N_{\text{array}} \max\{P_{c,\text{isolated}}\}} + 1 \tag{11}$$

where $\max\{P_{c,\text{isolated}}\}$ is the maximum absorbed power across all frequencies or periods experienced by an isolated WEC. The first term in the right hand side of Eq. (11) is the modified factor $q_{\text{mod}}$ defined by Babarit (2010) and addition of unity gives an effective magnification ratio. If $q < 1$, the average power captured by each WEC in the array is less than the power from an isolated WEC, which indicates that wave interactions have a negative effect on the power absorption in arrays. Conversely, the farm effect is regarded as constructive if $q > 1$.

## 3 Experimental comparison

The experiments were undertaken in the COAST wave basin at Plymouth University: 35 m long, 15.5 m wide with a depth of 1.0 m for these tests. Waves were generated by 24 hinged flap paddles at one end and there was an absorbing beach at the other giving a reflection coefficient of around 5 %. The device was moored from a small buoy connected by a light cord to the tank bed. Independent tests in the smaller 5 m wide flume in Manchester showed that the

results were almost unchanged when using a light horizontal tether. The standard pneumatic actuator or damper (Norgren Type RM/8016/M/100) used was almost linear, although the damping factor varied from one case to another. The force in the actuator was measured with a load cell (Omega LCMFD-10N) and the relative angle between column and beam $\theta_r$ was measured using an incremental shaft encoder (Wachendorrf 10000 PPR TTL). The damping factor was determined by post processing the damping moment assumed to be of the form

$$M_{\text{fit}} = B_0 + B_d \dot{\theta}_r + B_a \ddot{\theta}_r \qquad (12)$$

The least squares goodness-of-fit $R^2$ was always greater than 0.9 and generally around 0.95. An example of the time variation of moment at hinge $M_h$ is shown in Fig. 3. The inertial component was very small in relation to that due to body masses and is ignored in the numerical model.

The mass and inertia distributions for the system are shown in Table 1.

Figure 4 shows the variation of amplitude of complex relative rotation $|\theta_r|$ at the hinge and the CWR with wave period compared to the numerical model for $H \approx 0.03$ m; note that both $H$ and $B_d$ were different for each test and the numerical model used the experimental values for direct comparison.
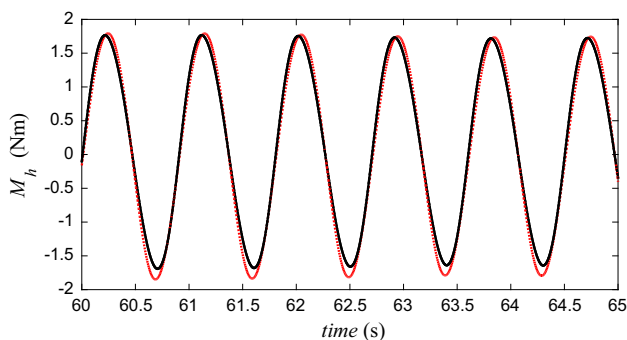


**Fig. 3** Example variation of hinge moment $M_h$ with time; $H \approx 0.05$ m and $T = 0.9$ s. The *full line* is from measured force and *dashed line* is fit by Eq. (12) ($R^2 = 0.96$)
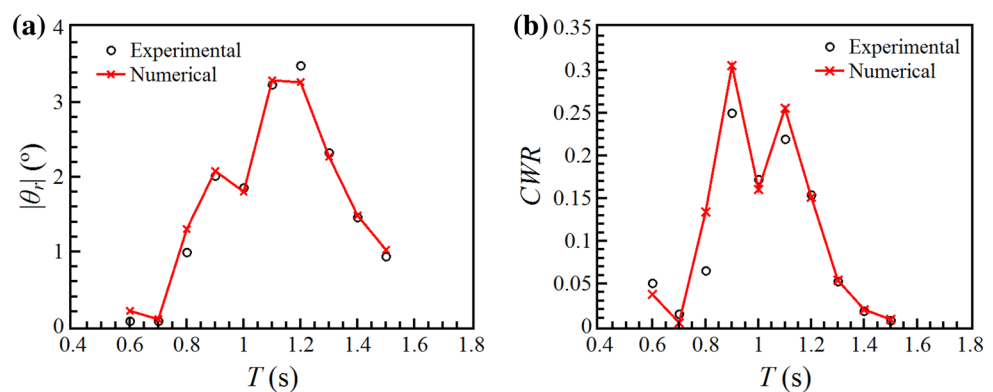
Values of $B_d$ are given below in Fig. 6a. For a typical swell period of 10 s the model scale is about 1:70 giving a full scale wave height of about 2 m. The prediction from linear diffraction theory can be seen to be reasonably close as might be expected for relatively small $H/\lambda$ and angular motion.

For $H \approx 0.05$ m (3.5 m full scale) the prediction of angular motion is still good but the CWR is generally somewhat overestimated as shown in Fig. 5. Nonlinear effects become more prominent as $H$ increases and have also been shown to reduce power and motion for a two-body vertically aligned system (Yu and Li 2013). Nonlinear effects may be inviscid, due to hydrostatic pressure and wave characteristics, or viscous, due to increasing drag effects. In addition, it should be noted that the angular motion is proportional to $H$ and the power to $H^2$, so relative differences may be expected to be greater for CWR which is a function of the power. This agreement indicates that the linear model is quite accurate for small $H$ conditions which would be typical of operational conditions.

## 4 Optimisation of damping and hinge point for power output

The damping factor of the pneumatic damper could not be varied in the experiments. However in a commercial system, whether hydraulic or direct drive, this can be controlled and it is valuable to determine optimum values for power generation for each period using the numerical model. Figure 6a shows the optimum values of $B_d$ at each wave period obtained from the linear diffraction analysis together with the actual experimental values for $H \approx 0.03$ and 0.05 m. The optimum value can be seen to vary considerably with period $T$ and the experimental values also vary, by coincidence both having minimum values at the same wave period. The CWR shown in Fig. 6b has increased from the previous maximum of ∼0.3 to 0.45 at $T = 1.16$ s where the optimised $B_d$ is 0.8 Nms. The corresponding angular motions in Fig. 6c are also seen to vary and the optimised condition have a maximum ampli-

**Fig. 4** For wave height $H \approx 0.03$ m, depth $d = 1.0$ m and post processed experimental damping factor $B_d$ for each case: **a** variation of amplitude of complex relative rotation $|\theta_r|$ with period $T$; **b** variation of capture width ratio (CWR) with period $T$

**Fig. 5** For wave height $H \approx 0.05$ m, depth $d = 1.0$ m and post processed experimental damping factor $B_d$ for each case: **a** variation of amplitude of complex relative rotation $|\theta_r|$ with period $T$; **b** variation of capture width ratio (CWR) with period $T$
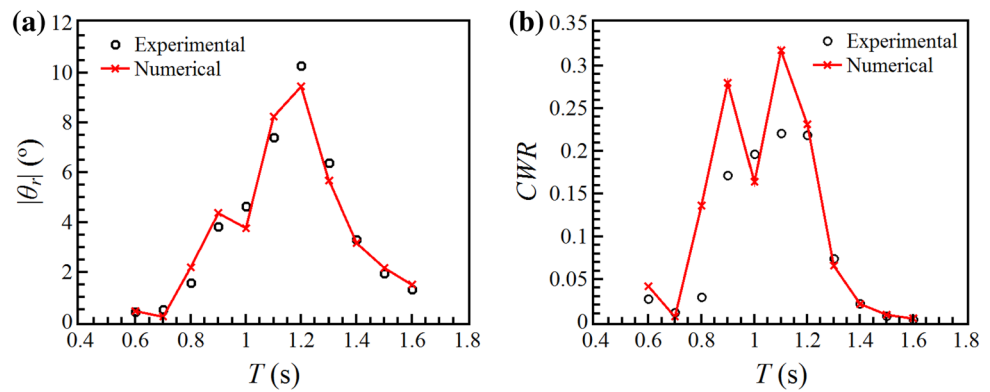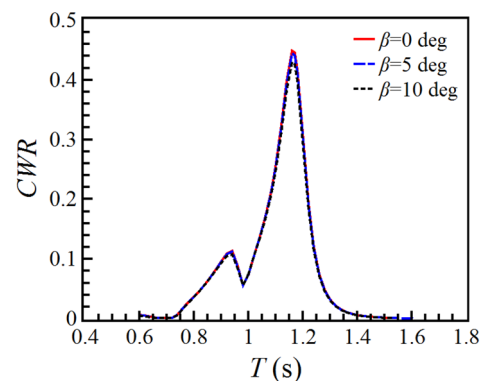


**Fig. 6** For wave height $H = 0.03$ m and $Z_h = 0.21$ m: **a** variation of experimental and optimum $B_d$ with period $T$; **b** Variation of capture width ratio (CWR) with period $T$ for optimum $B_d$; **c** Variation of amplitude of complex relative rotation $|\theta_r|$ with $T$ with optimum $B_d$
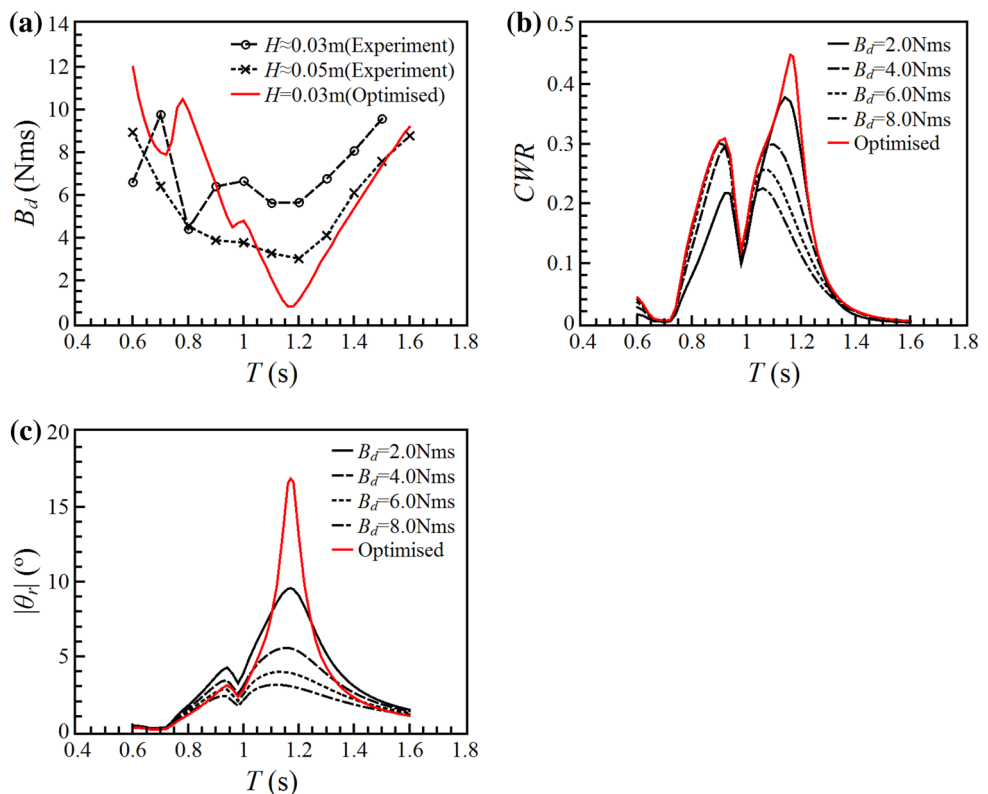


tude of about $17^o$. With such magnitudes nonlinear effects are likely to be significant as they were for the experimental conditions with $H \approx 0.05$ m. However the trends for optimising CWR with $B_d$ are likely to be valid, although magnitudes are likely to be reduced.

It has been assumed so far that the device is perfectly aligned with the wave incident angle $\beta$ and indeed this has been observed to be a close approximation in the experiments. In the numerical model the approach angle $\beta$ may simply be varied and Fig. 7 shows the CWR variation with wave period $T$ with constant $B_d = 0.8$ Nms for $\beta = 0, 5°$ and $10°$; there is negligible dependence.

Another parameter which is likely to influence the CWR is the vertical position of the hinge $Z_h$ (above still water level); for these tests $Z_h = 0.21$ m was used as the value previously



**Fig. 7** Variation of optimised capture width ratio (CWR) with period $T$ for $H = 0.03$ m, $B_d = 0.8$ Nms, $Z_h = 0.21$ m, depth $d = 1.0$ m and angle of incidence $\beta = 0, 5°, 10°$.

**Fig. 8** Effect of different $Z_h$ with $H = 0.03$ m, depth $d = 1.0$ m with $B_d$ optimised for each period: **a** variation of mean power $P_c$ with period $T$; **b** variation of capture width ratio (CWR) with period $T$; **c** variation of amplitude of complex relative rotation $|\theta_r|$ with period $T$; **d** variation of optimised $B_d$ with period $T$
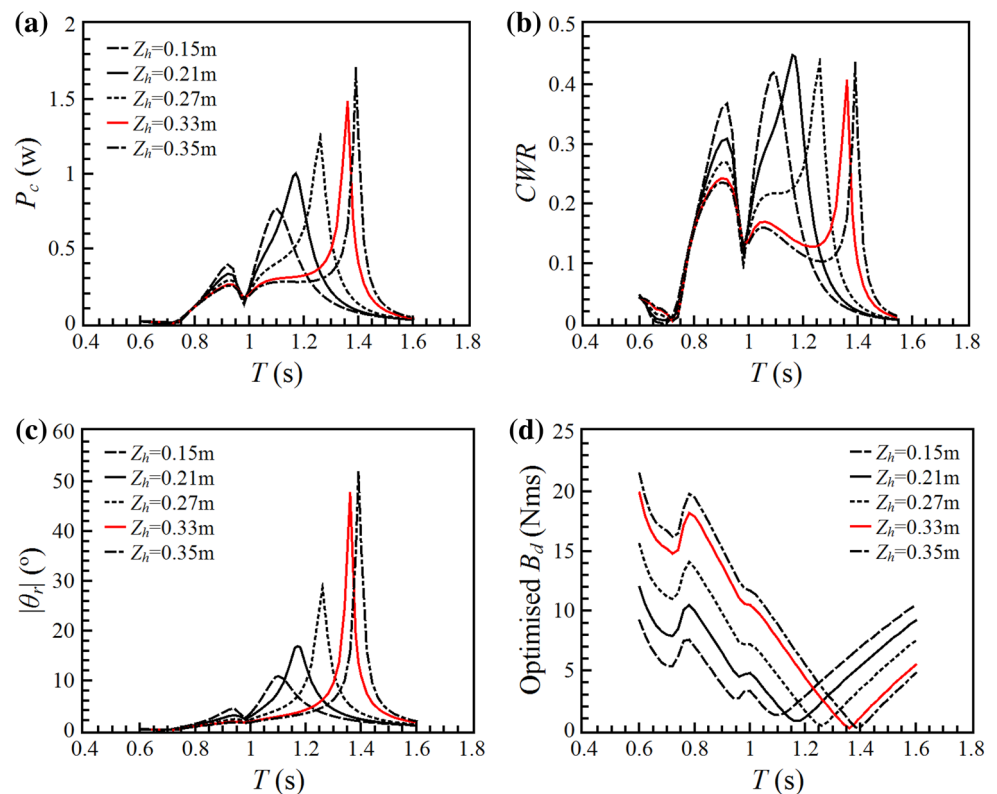


found experimentally to give near maximum power (with experimental therefore unoptimised $B_d$ values). This position will clearly influence the moment about the hinge and also the inertia. Raising the hinge will increase the moment which is desirable but also increase the inertia which may be undesirable. A range of values is now considered between 0.15 and 0.35 m and $B_d$ is varied to give optimum power. Results are shown in Fig. 8 based on $H = 0.03$ m with $B_d$ optimised for each $T$. Increasing $Z_h$ causes the maximum power to increase and occur at larger $T$ (Fig. 8a); the maximum CWR shows little variation as might be expected (Fig. 8b). The $B_d$ values show considerable variation as before (Fig. 8d). Figure 8c however shows that the relative rotation has now become very large, greater than 50° for $Z_h = 0.35$ m. Non-linear effects will certainly be important reducing CWR but again the trends of CWR with $Z_h$ are likely to be represented.

There are sharp dips in CWR around $T = 0.95$ s and peaks around $T = 0.85$ and 1.10 s in Figs. 6b, 7 and 8b. The resonant frequencies of relative pitch motion of floats in free response are identified to be 0.72, 0.99 and 1.13 s in Eatock Taylor et al. (2016). While the peak in CWR at $T = 1.1$ s approximately coincides, the peak at $T = 0.85$ s does not. The angle of rotation (from the horizontal) for the bow/mid float is in antiphase with that for the stern float for periods between 1.05 and 1.25 s and the relative phase increases from 180° for 220° for $T$ between 1.25 and 1.35 s, reducing rapidly for larger periods. For periods less than 1.05 s relative phase

changes rapidly from 270° at $T = 0.95$ s to 0 at $T = 0.7$ s with antiphase at $T = 0.85$ s coinciding with the peak in CWR. Clearly the coupled motion in waves is more complex than for floats in still water with excitation forces modifying the phase of pitch motion; surge forcing by waves for example is known to be significant (from model analysis in Stansby et al. 2015a), while there is no relevant surge resonant response. The established relatively simple connections between resonance and power amplification for single bodies is thus much more complex for multiple bodies emphasising the value of models such as that presented here which capture this complexity.

# 5 Row interaction

In practical applications wave energy devices will be deployed in arrays for significant electricity generation. Here we make a preliminary investigation with three and five devices arranged broadside in a row across the wave propagation direction. The layout of a five-device array with spacing of 1.0 m is shown in Fig. 9.

Figure 10 shows the variation of the array power factor $q$, defined in Eq. (11), with wave period for $\beta = 0$ and $B_d$ and $Z_h$ fixed at 0.8 Nms and 0.21 m respectively. Cross spacing between devices of 1, 2 and 4 m are in the range of about $0.5 \sim 2.0$ wavelengths at $T = 1.16$ s. Note the
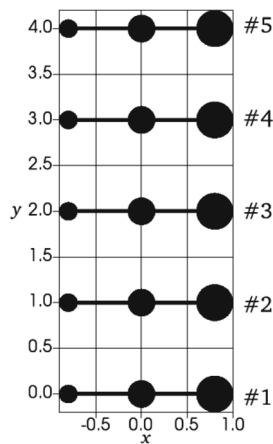
**Fig. 9** Five-device array with spacing of 1.0 m

device length between bow and stern float centres is 1.6 m. It can be seen that constructive and destructive effects change with wave period. Both constructive and destructive effects become more significant when there are more devices in the array. When there are five devices, the $q$-factor is up to 1.13 (constructive effect) at $T = 0.96$ s when the spacing = 4.0 m, and down to 0.705 (destructive effect) at $T = 1.17$ s when the spacing = 1.0 m. At the period of the maximum absorbed power ($T = 1.16$ s), the destructive effect is found when the spacing = 1.0 m. The constructive effect is found at $T = 1.16$ s when the spacing = 2.0 and 4.0 m, with a $q$-factor up

to 1.10 in five-device array (spacing = 2.0 m). With the spacing of 2.0 m the effect of incident wave direction is shown in Fig. 10 with the same $B_d = 0.8$ Nms and $Z_h = 0.21$ m. The magnification becomes smaller as incidence angle increases to 10°. These interactions are complex and the variation of power factor $q$ with period $T$ is markedly oscillatory at the lower wave periods ($T < 1.3$ s). The very small $q$ of 0.705 occurs with a spacing of 1.0 m which is probably too close in practical deployment. The farm effects are negligible for long waves ($T > 1.3$ s) where $q = 1$ (Fig. 11).

## 6 Discussion

The limitations of linear diffraction modelling based on potential flow analysis are well known but the way in which the accuracy and usefulness of the predictions decreases with increasing nonlinearity (in wave height and body motion) is problem specific. The problem considered here is quite complex with three floats each experiencing six modes of excitation although three are prominent: heave, surge and pitch in a vertical plane. Two of the floats are assumed to be rigidly connected and hinged to the third with a rotational damper to absorb power, making a two-body system. Validation of the linear modelling is achieved through comparison with controlled experiment and good prediction of the relative rotation is observed for regular wave excitation with

**Fig. 10** Variation of array power factor $q$ with period $T$ for spacings of 1.0, 2.0, 4.0 m, with $B_d = 0.8$ Nms, $Z_h = 0.21$ m, depth $d = 1.0$ m with row normal to wave direction ($\beta = 0$): **a** row of three devices and **b** row of five devices
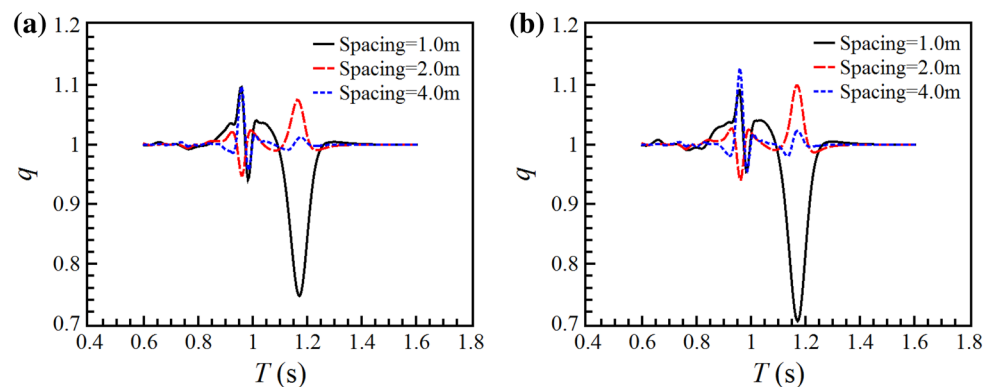


**Fig. 11** Variation of array power factor $q$ with period $T$ for spacing of 2.0 m with $B_d = 0.8$ Nms, $Z_h = 0.21$ m, depth $d = 1.0$ m for angles of incidence $\beta = 0, 5°, 10°$: **a** row of three devices and **b** row of five devices
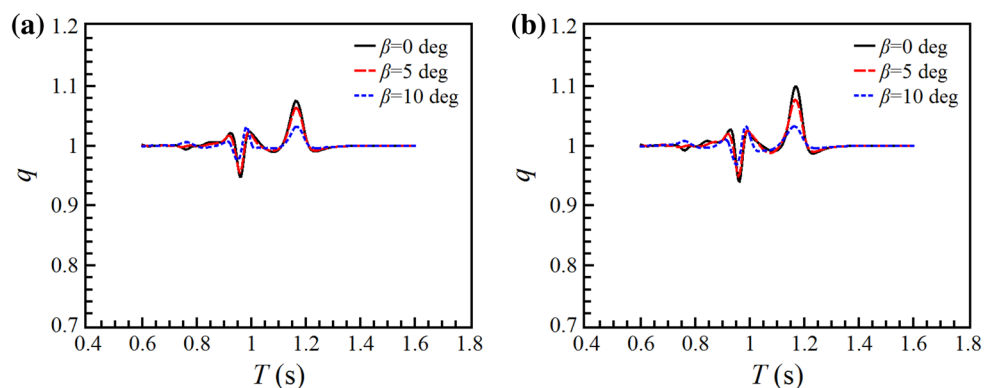
heights $H \approx 0.03$ and $0.05$ m ($H/\lambda \approx 0.01$ and $0.02$ at $T = 1.2$ s) with maximum amplitudes of relative rotation about $3.5°$ and $10.3°$. The average power absorbed is accurately predicted for $H \approx 0.03$ m but overestimated by up to 30 % for $H \approx 0.05$ m indicating a limit of accurate prediction. To relate to full scale, if we assume a representative period of 1.2 s for the experiments and a full scale swell period of 10 s, the model scale is about 1:70 and a 0.03 m wave height is equivalent to about 2 m full scale; this may be considered a representative magnitude for oceanic swell while smaller magnitudes occur in many situations. Note for irregular wind waves typical peak periods are 7–8 s which would give a model scale of around 1:40. The numerical model is thus directly useful for prediction. The linear damping factor for each period optimised for power capture shows considerable variation, with very high relative rotation with amplitudes up to $17°$. Clearly such predictions may not be accurate but within the context of a linear potential flow model may be compared with analytical values for the capture width ratio for an axisymmetric single point absorber in combined heave, pitch and surge. The maximum possible value is $3/2\pi \approx 0.48$, in combination of two modes (Falnes 2002), and here the maximum for M4 is 0.45. Importantly power capture has a narrow bandwidth for a point absorber while for this device with three floats it is broadband; the capture width ratio is greater than 0.2 for periods $+/-20$ % about a central value. It may be possible to improve this characteristic although the optimum shape of the capture width ratio versus period curve will probably be site specific. The practical magnitudes of capture width possible would require experimental assessment. Optimising power capture by varying hinge height causes even greater relative rotations, up to $52°$, which would be practically impossible as well as far beyond the limits for linear theory. Again however, the indicated trends in variation of power capture with this level are likely to be useful for optimisation. Interestingly as this height is increased the period for maximum power also increases indicating that a shorter, more compact, device may perform well.

In principle, a computational fluid dynamics (CFD) model incorporating all important physical characteristics and wave nonlinearity could be applied, but this would be massively expensive if indeed possible. In the present model there is the option of including a linearised representation of drag through a drag coefficient tuned to experimental results. In this study the rounded bases of the floats were assumed to provide very low drag and so the drag coefficient was ignored. There are additional nonlinear effects due to excitation forces which could be included. Also nonlinear buoyancy effects could be added but this requires knowledge of the free surface around a float which may not be known if there are significant diffraction and radiation interactions between floats. Overall, such partial improvements should be undertaken with caution. In contrast, application of the existing linear model to irregular and spread waves will enable further predictions and insights to be obtained in a straightforward manner.

In this model the horizontal motion is assumed to be small, as observed experimentally, and the mooring to have no effect. Experiments with and without a mooring buoy support the latter. However mooring loads and behaviour for both fatigue and extreme conditions need to be considered and the model should be developed further to include this. Efficient hydrodynamics for flexibly tethered floats in extreme and breaking waves has recently been developed (Lind et al. 2015) and will be applied to this relatively complex configuration.

The preliminary results for power capture in arrays are interesting and complex. The constructive effects in arrays with certain spacings and layouts warrants further study. These effects in irregular waves will certainly be less (Weller et al. 2010) but there is scope for increasing power capture.

## 7 Conclusions

The general frequency domain linear potential flow code DIFFRACT has been applied to the three-float (two-body) multi-mode broad-band wave energy converter M4 in regular waves through a multi-body dynamic model. Power is absorbed as a linear damper and good agreement has been shown with experiments for operational conditions. Such modelling is highly efficient and has enabled optimisation of the damping factor for power output, importantly showing strong frequency dependence. Power is generated due to relative angular motion between bodies at the hinge point above the mid float and the wave period for maximum power generation is shown to be dependent on vertical level, again optimising power by varying the damping factor. For the latter case in particular, rotations can be large and nonlinear effects reduce motion and power generation. Nevertheless the linear analysis indicates likely trends in capture width variation with both damping factor and hinge level which is valuable for optimisation. Results for a single row of 3 and 5 devices show that power is increased for certain spacings due to the multi-device interactions. Regular wave results are directly relevant to swell conditions which are prominent in certain regions as well as showing sensitivity of device characteristics to wave period. Present analyses of the wave energy converter in regular waves also provide insights for further investigations in random seas.

# References

Babarit A (2015) A database of capture width ratio of wave energy converters. Renew Energy 80:610–628

Babarit A (2013) On the park effect in arrays of oscillating wave energy converters. Renew Energy 58:68–78

Babarit A (2010) Impact of long separating distances on the energy production of two interacting wave energy converters. Ocean Eng 37:718–729

Eatock Taylor R, Taylor PH, Stansby PK (2016) A coupled hydrodynamic-structural model of the M4 wave energy converter. J Fluids Struct 63:77–96

Falcão AFO (2010) Wave energy utilization: a review of the technologies. Renew Sustain Energy Rev 14:899–918

Falnes J (2002) Ocean waves and oscillating systems. Cambridge University Press, Cambridge

Lind SJ, Stansby PK, Rogers BD (2015) Fixed and moored bodies in steep and breaking waves using SPH with the Froude Krylov approximation. J Ocean Eng Mar Energy. doi:10.1007/s40722-016-0056-4

Mei CC, Stiassnie M, Yue DKP (2005) Theory and applications of ocean surface waves. World Scientific, Singapore

Shabana AA (2010) Computational dynamics, 3rd edn. Wiley, Chichester

Stansby PK, Carpintero Moreno E, Stallard T, Maggi A (2015a) Three-float broad-band resonant line absorber with surge for wave energy conversion. Renew Energy 78:132–140

Stansby PK, Carpintero Moreno E, Stallard T (2015b) Capture width of the three-float multi-mode multi-resonance broad-band wave energy line absorber M4 from laboratory studies with irregular waves of different spectral shape and directional spread. J Ocean Eng Mar Energy 1(3):287–298

Stansby PK, Gu H, Carpintero Moreno E, Stallard T (2015c) Drag minimisation for high capture width with three float wave energy converter M4. In: Proc. 11th European wave and tidal energy conference (EWTEC 2015), Nantes, France

Sun L, Eatock Taylor R, Choo YS (2012) Multi-body dynamic analysis of float-over installations. Ocean Eng 51:1–15

Sun L, Eatock Taylor R, Choo YS (2011) Responses of interconnected floating bodies. IES J Part A Civil Struct Eng 4(3):143–156

Sun L, Eatock Taylor R, Taylor PH (2015) Wave driven free surface motion in the gap between a tanker and an FLNG barge. Appl Ocean Res 51:331–349

Weller SD, Stallard TJ, Stansby PK (2010) Experimental measurements of irregular wave interaction factors in closely spaced arrays. IET Renew Power Gener 4(6):628–637

Wolgamot H, FitzGerald CJ (2015) Nonlinear hydrodynamic and real fluid effects on wave energy devices. In: Proc I Mech Eng Pt A J Power Energy **(online 11 Mar 2015)**

Yu Y, Li Y (2013) Reynolds-averaged Navier-Stokes simulation of the heave performance of a two-body floating-point absorber wave energy system. Comput Fluids 73:104–114